Int. J. Electrochem. Sci., 14 **(2019)** 848 – 860, doi: 10.20964/2019.01.75

International Journal of
ELECTROCHEMICAL
SCIENCE
www.electrochemsci.org

Improved Lithium Storage Properties of the Reduced Graphene Oxide/Graphite Composites Based on Functional Groups Control Synthesis

Danhua Jiao[1,2], Zhengwei Xie[1,3], Qi Wan[1], Zhikai Wei[1], Xinxiu Yan[1,2], Faheem K. Butt[4], Meizhen Qu[1,]*

[1] Chengdu Institute of Organic Chemistry, Chinese Academy of Sciences, Chengdu 610041, PR China.
[2] University of Chinese Academy of Sciences, Beijing 100039, PR China
[3] Shenzhen New Hengye Battery Technology Co., Ltd., Shenzhen 518055, China
[4] Department of Physics, Division of Science and Technology, University of Education, College Road, Township, Lahore 54770, Pakistan
[*]E-mail: mzhqu18@cioc.ac.cn

Received: 5 October 2018 / *Accepted:* 12 November 2018 / *Published:* 30 November 2018

For lithium-ion batteries (LIBs), poor initial coulombic efficiency and poor cyclic performance of graphene oxide (GO) are facing great challenge in commercial application. This paper describes a class of active composites consisting of reduced graphene oxide (rGO) and graphite used as promising LIBs anodes. In addition to adjust the functional groups to decrease the irreversible capacity effectively, the construction of a conductive network between rGO and graphite synthesized during an ultrasonic process shortened the lithium ion migration path. The residual stable functional groups after thermal treatment also enhance the cyclic performance of the electrodes. Electrochemical test results revealed a high reversible Li-storage capacity of 446 mAh g^{-1} at 0.1 C (1 C=372 mAh g^{-1}), improved initial coulombic efficiency of 84.2% and superior cyclic performance with capacity retention of 93.8% after more than 400 cycles, showing great potential of this rGO/graphite anode material.

Keywords: lithium storage, graphene oxide, functional groups, initial columbic efficiency

1. INTRODUCTION

In currently available energy storage devices, LIBs are a promising power source. Their practical performance, however, is limited due to the chemical and physical structure of the battery components [1]. As the most commonly used anode material for LIBs, graphite is facing great challenge to improve its limited specific capacity (372 mAh g^{-1} theoretical specific capacity) [2,3]. Nowadays, there is an

imminent need to explore new anode materials for LIBs to meet the increasing demand of high specific capacity. As the precursor of graphene, GO is highly malleable and readily modified material provided with a higher specific capacity, which results from diverse oxygen-containing functional groups and double-layer charge storage. Unfortunately, GO-based materials often suffer from poor cyclic capabilities which come from undesirable conductivity; during initial cycling it bears a large irreversible capacity loss which leads to an initial coulombic efficiency of only ≈ 65% [4].

As a result, many groups are working to overcome these problems. rGO, derived from GO, has enhanced conductivity and regulated functional groups because that the partial functional groups removal in GO accelerates the charge carrier mobility; the stable and desirable amount of residual functional groups in rGO also could improve the rate capability and cycling behavior of electrodes. Thus the most important point is to find the association between the species and content of oxygen-containing functional groups and electrochemical properties though controlling its composition and stoichiometry is an arduous task [5,6]. Processing methods include chemical reduction, thermal reduction and the direct preparation of GO containing specific oxygen-containing functional groups. Considering the toxicity of reducing agents involved with the chemical reduction process, thermal reduction is a universally accepted way to obtain rGO [7,8]. Generally speaking, redox reactions of graphene oxide often occur at specific functional groups even if the existence of other specific functional groups contributed to additional reversible capacity. Thus the preparation of rGO with reversible functional groups is very significant. Preparing thermally rGO by partially adjusting the temperature while retaining some specific capacity-contributing functional groups still remains a challenge and the relationship between functional groups and the electrochemical propreties of GO-based materials is not be concluded so far. Numerous works are devoted to find the relationships. Wang et al. reported GO materials with introduction of epoxide and they explained that the epoxide group is beneficial to increase the first discharge capacity [9]. A conclusion was obtained by Kerisit that hydroxyls were found to affect negatively the capacitance, whereas the effect of epoxides was much less pronounced [10]. In addition, carboxyl groups were thought by Liu et al. to be advantageous to enhance capacitance capability of GO-based materials [11]. In short, there has not been a unified conclusion between functional groups and specific reversible capacities so far and poor initial coulombic efficiency resulting from the mass irreversible specific capacity formation still impedes the application of GO.

In this work, we reported a new rGO/graphite composite for LIBs anode material, which was synthesized via a facile and environmental-friendly thermal treatment. This method avoids harsh environmental conditions such as high temperature, inert atmosphere as well as a large amount of a toxic reducing agent and promotes the effective construction of conductive network between rGO and graphite. Furthermore, it preserves the stable and desirable amount of functional groups which are in favor of decreased irreversible specific capacities and improved cyclic performance for LIBs anode materials. The evolution of the functional groups during reduction was also investigated.

2. EXPERIMENTAL

All chemical reagents were analytical grade (purchased from Kelong Chemical Reagent Crop.

Chengdu, China) and used without further purification. The modified Hummer method was used to obtain graphene oxide (GO) using natural graphite flakes with a refined purity of approximately 200 mesh (Changsha Shenghua Research Institute, 99.999%) and graphite was used without any additional purification [12]. The Hummer method characteristically utilizes potassium permanganate ($KMnO_4$), hydrogen peroxide solution (H_2O_2) and concentrated sulfuric acid (H_2SO_4) in a multi-step, single vessel oxidation reaction [13].

The GO/graphite (GG) composite was prepared in advance: Firstly, a stoichiometric amount of GO and graphite was sonicated in deionized water using a cell crusher for 1 h to get a stable dispersion. Next, water was evaporated using a 70 ºC water bath and the final slurry was dried at 80 °C under vacuum. Samples with different reduction capabilities were obtained after annealing the GO/graphite composites at temperatures ranging from 130-160 ºC for 2 h in air atmosphere. The ratio of rGO and graphite was 8:92 and the samples treated at 130 °C, 140 °C, 150 °C and 160 °C were denoted as GG-130, GG-140, GG-150 and GG-160, respectively. GG was denoted as GO/graphite composite without thermal treatment.

The morphology of prepared samples was determined by scanning electron microscopy (SEM) [INCA PentaFETx3] and transmission electron microscopy (TEM) [JEM-100 CXJEOL]. The structure was characterized by X-ray diffraction (XRD) [X'Pert MPD DY1219, Cu Kα radiation λ=1.5406 Å] at room temperature. The composition of composites was investigated by thermogravimetric analysis (TGA) [NET-ZSCH, measured at a heating rate of 5 ºC min^{-1} in a nitrogen atmosphere]. X-ray photoelectron spectroscopy (XPS, PHI5600 Physical Electronics) investigations were performed to analyze carbon peak assignments and elemental composition [Al/Kα radiation; $h\upsilon$=1486.6 eV]. The samples were mixed with KBr and finely ground to produce pellets for the FT-IR measurements.

The electrochemical properties of GGs composites as LIBs anodes were evaluated via galvanostatic charge/discharge experiments (NEWARE 4000 A, Shenzhen, China), which were conducted on an automatic unit under different current densities from 0.01 to 3.0 V vs. Li/Li^+ at 25 ºC. Lithium metal was used as the counter electrode. 1.0 M $LiPF_6$ solution was used as electrolyte (purchased from Capchem. Technology Co., Ltd.), the solution was composed of dimethyl carbonate, ethylene carbonate and diethyl carbonate (1:1:1 in Volume). The entire process was performed in an argon-filled glove box. Electrochemical impedance spectroscopy (EIS) and Cyclic voltammograms (CV) tests were conducted on a PGSTAT302N Electrochemical System (AUTOLAB, USA) at an input signal of amplitude 5 mV (vs. OCP) and a frequency ranging from 100000 Hz to 0.01 Hz and a scan rate of 0.1 mV s^{-1}. Specific capacities were computed based on the active-layer mass (GGs) excluding conductive and binder additives.

3. RESULTS AND DISCUSSION

Fig. 1a confirms the reversible charge/discharge curves for the first cycle at 0.1 C (1 C = 372 mAh g^{-1}); commercial graphite and GG electrodes were used as the reference samples (detailed data is shown in Table 1). As seen in Table 1, the charge capacity of GG composites was 397 mAh g^{-1}, that is 1.19 times than graphite (331 mAh g^{-1}), indicating the high specific capacity contribution of GO. After

thermal treatment, the charge capacity increases to 446 mAh g^{-1} for GG-150, that is higher about 50 mAh g^{-1} than GG electrode. When the temperature exceeds 150 ºC, the first charge capacity of GG-160 electrode declines due to the disintegration of some specific functional groups. In addition, the first discharge capacities of GG-130- GG-160 electrodes continuously decrease comparing with GG electrode, and clearly rationalization that the excess capacity comes from the functional groups of GO. At the same time, the initial coulombic efficiency (CE) of thermal treated GGs electrodes significantly increases, especially for the GG-160 electrode (85.8%), which is almost comparable to commercial graphite and far higher than the 50-68% reported in the literature associated with GO-based electrodes [4,14,15]. As displayed in Table 1, the initial coulombic efficiency of GO is only 25%, which is hindering its commercial applications greatly. Though enhanced lithium storage capacities was provided with GO/graphite composite, the initial coulombic efficiency of 67.8% is still limited for LIBs anodes materials, and the large proportion of GO content leads to a waste of resources. Including the graphite/GO/carbon nanotube (GGCC) composite, the initial coulombic efficiency of it is merely 59.4%, the same with rGO/porous Si composite. The superior lithium storage capacity of GO has been well accepted universally, thus the high specific capacity could be easily obtained by adjusting the proportions of GO content. However, the large irreversible capacity during the first charge/discharge cycle is occupying a crucial role in the GO anodes applications. In other word, to enhance the initial coulombic efficiency of GO anodes is very important. In this paper, 85.8% of initial coulombic efficiency of GG-160 was provided after functional groups controlling synthesis, which is higher almost 13% than GG electrode. This indicates that the irreversible capacities of GO anodes can be decreased effectively by this facile method, which will promote the commercial applications of GO materials to a large degree. And this was never reported before. The unique electrochemical performance may be ascribed to the unstable functional groups removal from the GO surface that decreases the irreversible capacity effectively [16].

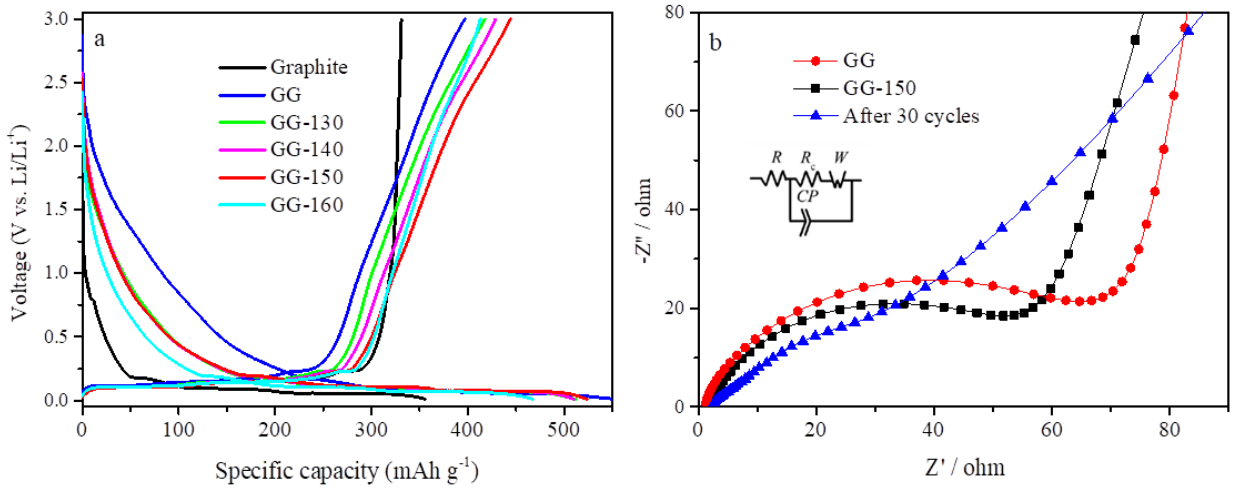

Figure 1. (a) The first charge/discharge profiles and (b) Nyquist plots of GG samples treated at different temperatures, equivalent circuits are shown in inset.

Table 1. Electrode data and fitted parameters from the equivalent circuit.

Electrode	R (Ω)	R_c (Ω)	1st CC (mAh g^{-1})	1st DC (mAh g^{-1})	1st CE (%)
Graphite	-	-	331	356	92.9
GG	1.35	50	397	554	71.7
GG-130	-	-	415	528	78.6
GG-140	-	-	432	525	82.3
GG-150	1.27	38	446	530	84.2
GG-160	-	-	413	481	85.8
After 30 cycles	2.01	30	358	340	99.4
GO [4]	-	-	350	1400	25.0
Graphite/GO [15]	-	-	704	1039	67.8
GGCC [4]	-	-	1153	1942	59.4
rGO/porous Si [14]	-	-	1695	2463	68.8

To further understand the conductivity of different materials, the EIS of GG, GG-150 electrodes and GG-150 after 30 charge-discharge cycles were performed. All Nyquist plots possess a depressed broad semicircle at the charge-transfer to kinetically controlled region at higher frequencies and a straight line at low frequencies for the mass-transfer-controlled Warburg region [17]. An equivalent circuit is shown in the inset of Fig. 1b and the fitting parameters are found in Table 1; R denotes the resistance of electrolyte for the electrochemical system and R_c denotes charge-transfer resistance. The constant phase element (*CP*) normally indicates the double layer capacitor while W is the Warburg element [18]. As shown in Fig. 1b, GG maintains a superior electrical conductivity due to the secondary ball milling, uniform dispersion in the ultrasonic process and more inlets/outlets for the deintercalation/intercalation of lithium ions [19]. After thermal reduction, GG-150 becomes smaller with R_{ct}, suggesting an inverse relationship between electrical conductivity and the number of functional groups. We also find that the R_{ct} of GG-150 electrode is 38 Ω and it decreases to 30 Ω after 30 charge/discharge cycles. This could be ascribed to the reduction of functional groups during the charge/discharge process. Combining the electrochemical performances of both the GG and GG-150 electrodes, a positive correlation is suspected between the conductivity and the initial coulombic efficiency.

TGA was used to investigate the composition after thermal treatment. These experiments were performed from room temperature to 600 ºC (heating rate 5 ºC min^{-1}) under a nitrogen atmosphere. As shown in Fig. 2a, the curves display two degradation steps of GG-130-GG-160 samples and three degradation steps of GG sample. The stable chemical stabilities of GG-130-GG-160 samples can be contributed to the partial oxygen removal under thermal treatment. The first step is ascribed to absorbed water on the surface of GGs samples at approximately 20 ºC with water percentages ranging from 9-12%. The second step at 120 ºC comes from the loss of epoxy and hydroxyl groups as well as any remaining water molecules [20]. The total weight losses are 1.5%, 1.9%, 2.3% and 2.6% for samples prepared at 160 ºC, 150 ºC, 140 ºC, and 130 ºC, respectively. This indicates that the content of functional groups decreases as the thermal reductive temperature of graphene oxide increases. At temperatures above 150 ºC, the slope steepens due to decomposition of some specific functional groups; this may

explain the sudden drop of specific capacity of the GG-160 sample. The third step of GG at 320 ºC derives from some functional groups decomposition at high temperature, this dissociation may be beneficial to the stable performance of GGs samples after thermal treatment.

The structures were determined by XRD, the corresponding results are illustrated in Fig. 2b. The XRD patterns of the GG composites are similar to pure graphite without any other phases, indicating a high purity of GG composites is achieved. The characteristic peak of GG composites located at approximately 26.24º which belongs to the (002) plane of natural graphite appears as a slight blue shift and the intensity weakens as the temperature increases [21]. As previously reported, the characteristic peak at 24º belongs to rGO which might be the reason why the peak at 26.24º shifts to the left [22]. In addition, the reduced peak intensities are likely ascribed to the decreased quantity of functional groups and GO content in the composites which results from thermal reduction. Both narrow and sharp peaks suggest a larger size with a crystalline grain. Fig. 2c gives the Raman spectra of GG treated at different temperatures as well as the spectrum of bare graphite. The peak located ~1360 cm^{-1} (D peak) corresponds to the defects and disorder in the hexagonal graphitic layers or edges and the center peak at 1580 cm^{-1} (G peak) corresponds to the vibration of sp^2 bonded carbon atoms [9]. GG-130, GG-140, GG-150 and GG-160 samples all exhibit similar characteristic peaks. The Raman D to G band intensity (I_D/I_G) ratio of rGO is often used to determine the amount of disorder in GO [23]. As shown in Fig. 2c, the I_D/I_G increases as compared with GG and this may be ascribed to additional active sites in rGO [24]. When absorbed water is removed and the labile functional groups decompose, the value of I_D/I_G decreases; a conclusion supported by TGA results.

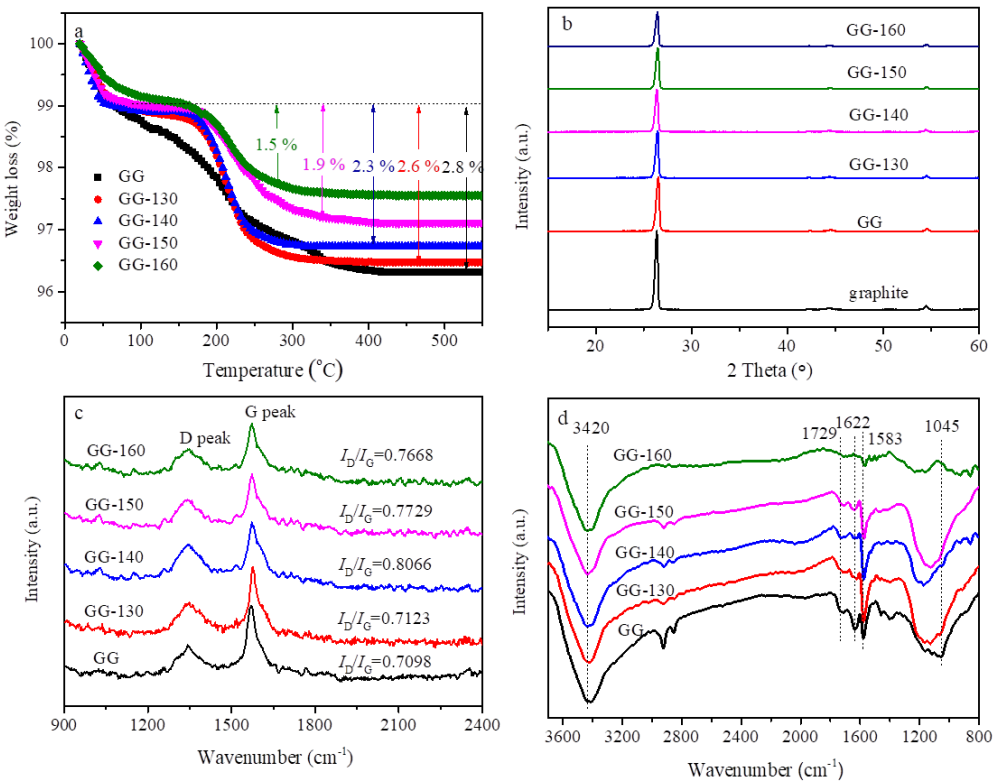

Figure 2. (a) TGA, (b) XRD, (c) Raman and (d) FTIR spectra of GG composites.

The FTIR spectra shown in Fig. 2d gives the characteristic peaks of GGs composites. The dominant absorption band located at 3420 cm^{-1} is ascribed to -OH peaks from H_2O and COOH, absorption peaks at 1729 cm^{-1}, 1622 cm^{-1} and 1583 cm^{-1} were assigned to the C=O stretch of COOH, lactone and aromatic C=C bonds. When the carbonyl group is conjugated with the benzene ring, the aromatic ring peak at 1620 cm^{-1} splits with a new absorption peak appearing at 1580 cm^{-1}. The absorption peak at 1045 cm^{-1} is ascribed to C-O stretches from C-OH and epoxides [25,26]. As shown, thermal reduction at 130 °C clearly lowers the intensity of the 3420 cm^{-1} peak without altering other peaks from the GG composites, indicating that dissociation of intercalated and adsorbed water of GO is the primary transformation. The overlapped bands from 1100-1280 cm^{-1} are ascribed to peroxide, anhydride, ether and epoxide groups [27]; these significantly increase from 130-140 °C but decline at 150-160 °C and the changing trend is coincide with I_D/I_G ratio values. As the treatment temperature increases, the intensity of epoxide peak at 1058 cm^{-1} decreases while the C=O peak slightly increases. This indicates the epoxide is very unstable under thermal treatment while the C=O groups are more stable. When the temperature exceeds 150 °C, the peaks located at 1720 cm^{-1} and 1620 cm^{-1} almost completely disappear, which suggests the carboxyl group decomposition. These results are also consistent with TGA and Raman results.

X-ray photoelectron spectroscopy (XPS) was conducted to investigate the chemical composition of GGs composite. The spectra of C1s in Fig. 3 suggest the existence of four dissimilar components with binding energies of 284.4, 286.5, 287.3, 288.2 and 289.5 eV; these correspond to the graphitic C=C/C-C, C–OH, C-O-C, C=O and O–C=O bonds, respectively [28], and agree well with Raman results (that oxygen functional groups remain after thermal treatment). The fitted parameters are shown in Table 2. Comparing the results of GG and GG-130, a suspension can be obtained that the epoxide, carbonyl and carboxyl groups are less stable as their residual amounts decrease a lot after thermal treatment at low temperature but hydroxyl groups display an opposite tendency. Generally speaking, dissociation of both intercalated and adsorbed water in GO often occurs below 100 °C and would lead to the lowering of the broad hydroxyl peak. As a result, we have reason to believe that epoxide, carboxyl and carbonyl groups can easily be reduced to hydroxyl groups during thermal treatment and explains the increase in the intensity of the hydroxyl groups. As the thermal treatment temperature increases, hydroxyl and epoxide groups decline but the carbonyl and carboxyl groups increase with the carboxyl groups plateauing at GG-150, higher than GG composites. TGA results indicated that labile functional groups decompose at high temperatures, the intensity of the carboxyl groups decreases at or above 160 ºC, and the GG composites also show the best electrochemical performance of GG-150 electrode. So, we speculate that the carboxyl may perform a constructive role in the reversible capacity. These results indicate that epoxide and carbonyl groups are readily reduced, more so than other oxygen-containing functional groups. Because these two groups possess the greatest degree of reduction as compared with GG and applies to rGO obtained by any method. Combining the GG samples with different thermal temperatures, an obvious result is the continual decrease of epoxide and hydroxyl group peaks with a concomitant increase in the intensities of carboxyl and carbonyl groups. It is also interestingly noteworthy that the layered structure of GO bears epoxides and hydroxyls on basal planes, whereas carboxyl and carbonyl on the edge [29]. This may explain the problem of interlayer stacking of thermal treated samples as well as the procedure in charge and discharge reactions. These results are all consistent with Raman results.

We speculate that our thermal treatment method improves initial coulomb efficiency by enhancing the conductivity; carboxyl amounts may perform a helpful role in the lithium storage capacity and epoxide may play an significant role in the initial coulombic efficiency of samples.

The first two curves for charge/discharge of GG and GG-150 electrodes at a constant current of 0.1 C are displayed in Fig. 4a; the shapes of the two electrodes shapes are similar. GG-150 and GG show 446 mAh g^{-1} and 397 mAh g^{-1} of the first charge capacity and 530 mAh g^{-1} and 554 mAh g^{-1} of the first discharge capacity, respectively. This implies a close association among the functional groups of GO and the specific capacity of materials. The quantitative irreversible capacity in the second charge capacity is often related to the creation of an SEI (Solid electrolyte interphase) film in the first cycle, which occurred above 0.5 V [30].

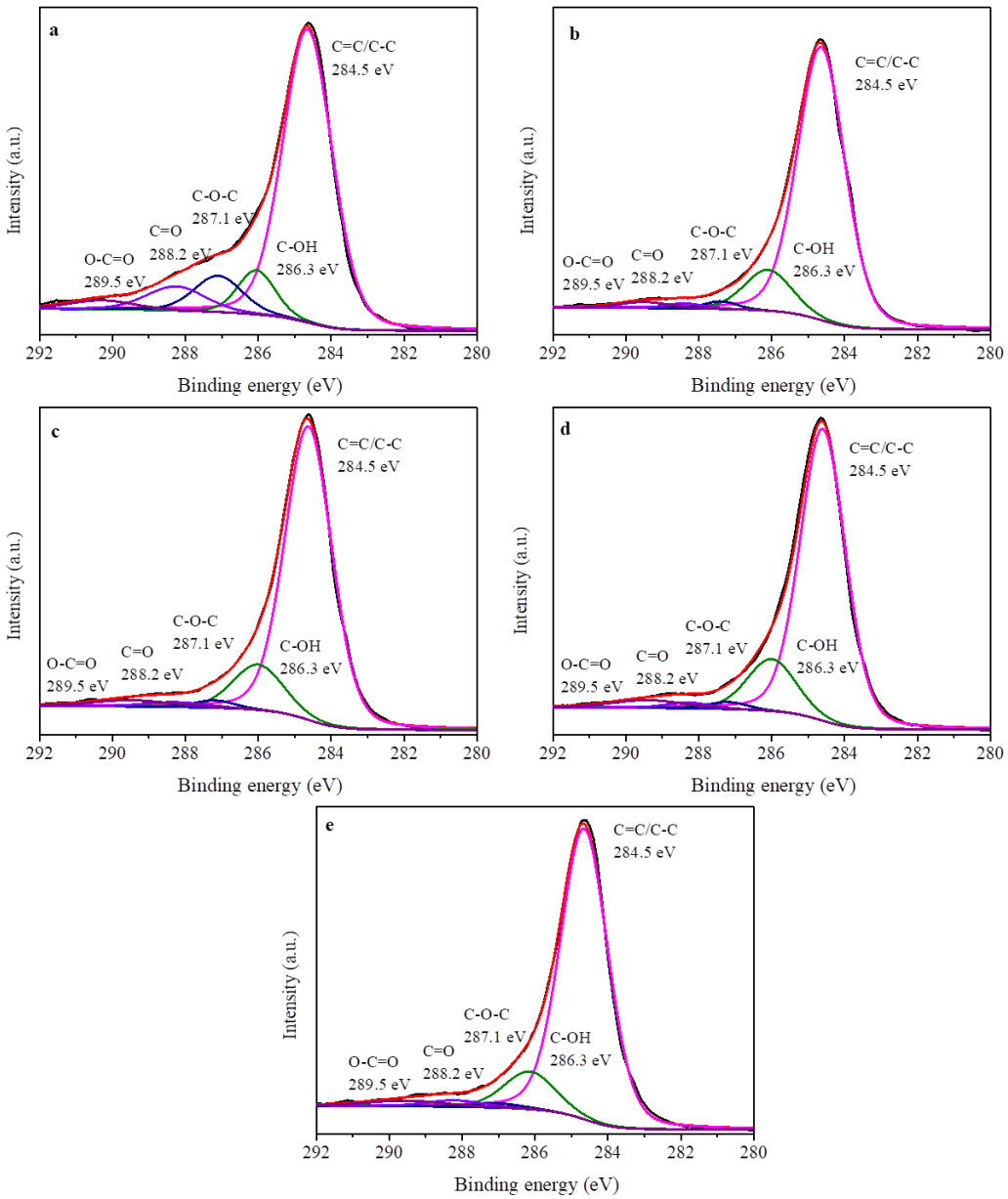

Figure 3. Fitting results of C1s spectra of the GG treated at different temperatures (a, GG; b, GG-130; c, GG-140; d, GG-150; e, GG-160)

There are also some lithium side reactions during this process. As seen in the figure, the specific capacity of GG-150 in second discharge profile is larger than GG, and can be attributed to the stable and desirable amount of residual oxygen in rGO. However, there a slight difference between the lithium storage modes for GG-150 and GG. The process of lithium intercalation into graphene oxide sheets occurs below 0.5 V [31]. It is noteworthy that the excess capacity of GG-150 appears from 0.1-0.25 V. This further confirms the contribution of controllable oxygen functional groups via thermal treatment. The elongated plateau of ≈ 0.1 V can be explained from the graphite space intercalation. In contrast, in the voltage window range of 0.1-0.5 V, the slope of GG-150 electrode is shorter than that of GG during the second discharge curve. This phenomenon confirms that the heat treatment procedure produces stacking sheets of graphene oxide and confirms results from Raman spectra. Fig. 4b gives the CVs of GG and GG-150 electrodes (scan rate of 0.1 mV s^{-1}; voltage window from 0.01 V to 3.0 V vs. Li/Li^+). The faded peaks from 2.2 V to 0.5 V of GG-150 in the second cycle conform to the creation of an SEI film and desorption of water or reduction of surface groups which are only observed during the first cycle [32]. The large cathodic peaks of GG-150 at 2.1 V and 1.5 V may be attributed to the Li-intercalation with the surface groups [33]; they also diminish significantly during the second cycle due to partial reduction of GO and never could be found with GG electrode. Combining with XPS results, this may explain the some increased oxygen-containing functional groups content of GG-150 electrode, carbonyl and carboxyl groups are suspected.

Table 2. Elements of the XPS with fitted parameters for GG.

Sample	C=C/C-C	C-OH	C-O-C	C=O	O-C=O
GG	72.86	8.35	8.74	7.15	2.90
GG-130	81.40	13.32	2.19	1.13	1.96
GG-140	81.58	12.50	1.72	1.46	2.74
GG-150	81.85	11.89	1.39	1.52	3.35
GG-160	82.77	11.34	1.15	2.15	2.59

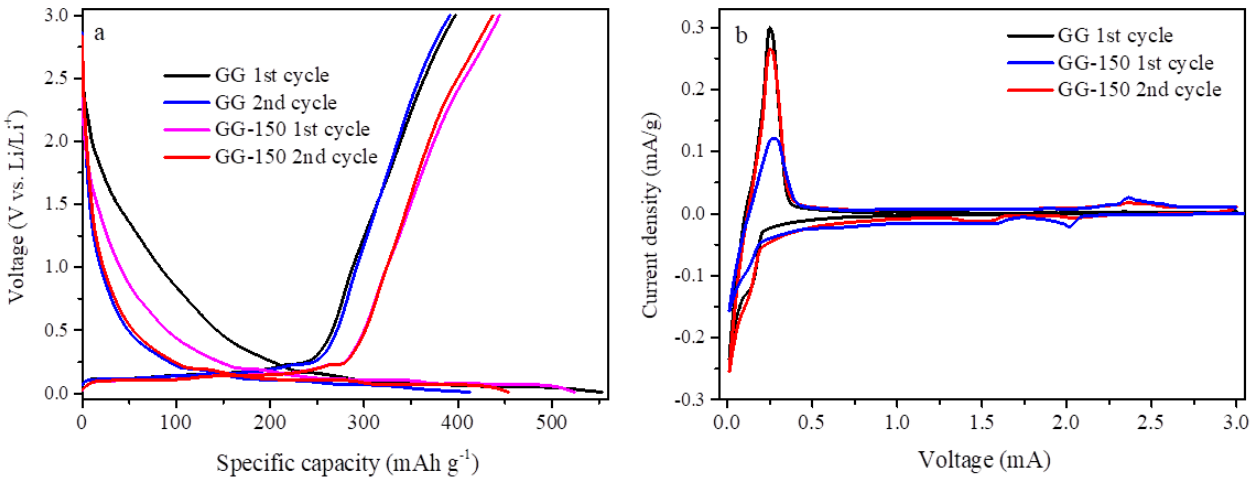

Figure 4. First and second charge/discharge outlines cycled from 0.01 V to 3.0 V (vs. Li/Li^+): (a) GG and GG-150; (b) the first and second relevant CVs of graphite and GG-150

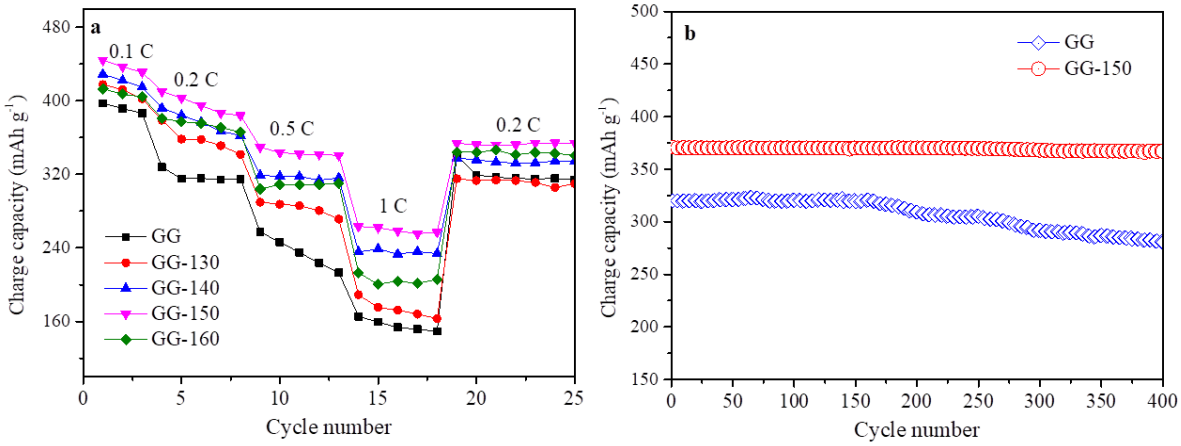

Figure 5. (a) Rate capability of GG composites; (b) cyclic performance of GG and GG-150

The rate capability of GG composites at dissimilar current densities are shown in Fig. 5a. Generally, the thermally treated rate capabilities of GGs electrodes are invariably superior to untreated GG sample and they increase with temperature. Tangibly, the initial charge capacity of the GG-150 sample is 446 mAh g^{-1} at 0.1 C; as the current density increases, so does the charge capacity and its higher than the other electrodes, though it drops slightly. At a current density of 1 C, the charge capacity of the GG-150 electrode reached to 253 mAh g^{-1}; this is 110 mAh g^{-1} higher than GG electrode. Once the current density returns to 0.2 C, the charge capacity of GG-150 could even increase to 358 mAh g^{-1}. These outcomes give an outstanding rate performance of rGO/graphite composites. The cyclic performance of this electrode was confirmed by way of the capacity retention of GG-150, which remained at 93.8% (Fig. 5b) after more than 400 cycles. While the capacity retention of GG composite is only 85.2% and the specific capacity of it decreases sharply after 160 cycles. The better performance of GG-150 electrode can be ascribed to the stable and desirable amount of residual oxygen groups after thermal treatment. And it is worth noting that all cyclic performances were conducted after rate performance measurements.

The superior electrochemical performance of GG-150 electrode is depicted in Scheme 1. Due to the various stoichiometries and structures of GO derived from different oxidation contents and preparation methods, GO is often divided into small in-plain aromatic domains. As illustrated in Scheme 1, graphite is well coated by GO, benefiting from the ultrasonic procedure to shorten the lithium transmission pathway. In addition, thermal treatments removed unstable functional groups such as hydroxyls, epoxides including adsorbed water. As a result, the higher reversible capacities and higher initial coulomb efficiency of GGs electrodes are ascribed to the stable and desirable number of functional groups, derived from the improved conductivity [16].

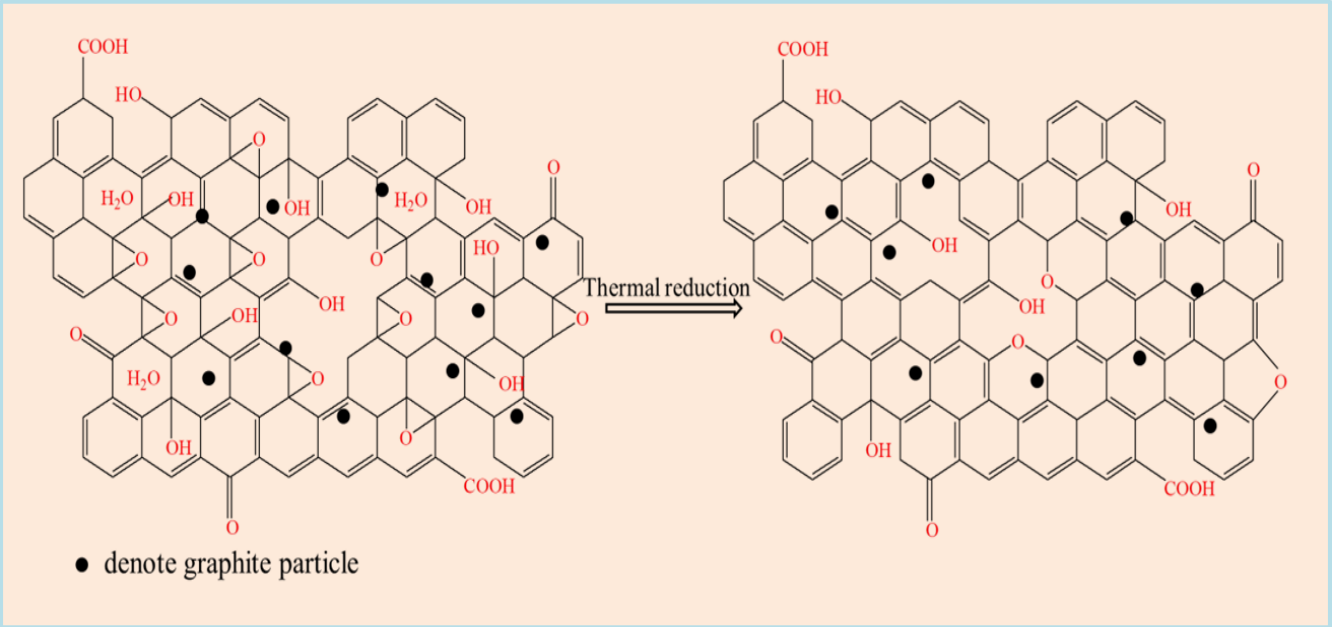

Scheme 1. Progression of GG functional groups during thermal treatment

4. CONCLUSIONS

The rGO/graphite composites were prepared via ultrasonication and a thermal reduction method at low temperatures. Characterization results confirmed the construction of a conductive network between graphite and rGO and showed outstanding conductivity with a mechanical buffer during the charge/discharge procedure as well as a short lithium transmission pathway. Thermal treatment removed the unstable functional groups and the stable and desirable amount of residual oxygen groups positively contributed to the superior initial coulombic efficiency; this effectively reduced the irreversible capacity and was beneficial for improved cyclic performance. Furthermore, the number and variety of functional groups on the rGO surface were effectively regulated by changing the thermal treatment temperature. As an anode material for LIBs, the GG-150 composites exhibited a commercially applicable initial coulombic efficiency of 84.2%, exceptional cyclic performance with capacity retention of 93.8% after more than 400 cycles, and a superior rescindable capacity (446 mAh g^{-1}). We also observed that epoxide, carboxyl and carbonyl groups were readily reduced to hydroxyl groups at low temperature. Epoxide and carbonyl groups were more readily reduced than other oxygen-containing functional groups. In addition, we speculated that the increased carboxyl amounts might improve storage capacity while epoxide might act as a negative role in the initial coulombic efficiency. These results are of great significance in the purposeful construction of anodes with exceptional specific capacities and decent initial coulombic efficiency. In general, we believe that the rGO/graphite electrode has a great potential to be accepted as anodes for LIBs with superior initial coulombic efficiency and considerable cyclic performance.

ACKOWLEDGEMENTS
This study was completed with the help of National Natural Science Foundation of China (grant no.51474196) and Sichuan Provincial science of Technology department project (grant no. 2017GZ0114). For the meantime, our appreciation went to Analytical and Testing Center of Chengdu Branch, Chinese Academy of Sciences.

References

1. V. Etacheri, R. Marom, R. Elazari, G. Salitra and D. Aurbach, *Energ. Environ. Sci.*, 4 **(**2011) 3243.
2. C.H. Hsu, H.H. Lin, Y.H. Liu and H.P. Lin, *New J. Chem.*, 42 **(**2018) 9058.
3. Y.G. Huang, X.L. Lin, Q.C. Pan, Q.Y. Li, X.H. Zhang, Z.X. Yan, X.M. Wu, Z.Q. He and H.Q. Wang, *Electrochimi. Acta*, 193 (2016) 253.
4. J.X. Zhang, Z.W. Xie, W. Li, S.Q. Dong and M.Z. Qu, *Carbon*, 74 **(**2014) 153.
5. T. Szabo, O. Berkesi, P. Forgo, K. Josepovits, Y. Sanakis, D. Petridis and I. Dekany, *Chem. Mater.*, 18 **(**2006) 2740.
6. S.D. Dabhi, S.D. Gupta and P.K. Jha, *J. Appl. Phys.*, 115 **(**2014) 171.
7. Y.B. Kang , X. Yu, M, Kota and H.S. Park, *J. Alloy. Compd.*, 726 (2017) 88.
8. X.K. Zhang, P. Wu, L. Jiang, X.F. Zhang, H.X. Shi, X.S. Zhu, S.H. Wei and Y.M. Zhou, *Appl. Surf. Sci.*, 444 **(**2018) 448.
9. Wang D.W., Sun C.H., Zhou G.M., F. Li, L. Wen, B.C. Donose, G.Q. Lu, H.M. Cheng and I.R. Gentle, *J. Mater. Chem. A*, 1 **(**2013) 3607.
10. S. Kerisit, B. Schwenzer and M. Vijayakumar, *J. Phys. Chem. Lett.*, 5 (2014) 2330.
11. Y. Liu, R.J. Deng, Z. Wang and H.T. Liu, *J. Mater. Chem.*, 22 **(**2012) 13619.
12. D.X. He, W.D. Xue, R. Zhao**,** W.C. Hu, A.J. Marsden and M.A. Bissett, *J. Mater. Sci.*, 53 **(**2018) 9170.
13. Y.C.G. Kwan, G.M. Ng and C.H.A. Huan, *Thin Solid Films*, 590 **(**2015) 40.
14. L.S. Jiao, J.Y. Liu, H.Y. Li, T.S. Wu, F.H. Li, H.Y. Wang and L. Niu, *J. Power Sources*, 315 **(**2016) 9.
15. J.X. Zhang, H.Q. Cao, X.L. Tang, W.F. Fan, G.C. Peng and M.Z. Qu, *J. Power Sources*, 241 (2013) 619.
16. X. Zhang, S.C. Han, P.G. Xiao, C.L. Fan and W.H. Zhang, *Carbon*, 100 **(**2016) 600.
17. X.L. Yu, C.Z. Zhan, R.T. Lv, Y. Bai, Y.X. Lin, Z.H. Huang, W.C. Shen, X.P. Qiu and F.Y. Kang, *Nano Energy*, 15 **(**2015) 43.
18. K.J. Zhang, H.B. Wang, X.Q. He, Z.H. Liu, L.Wang, L. Gu, H.X. Xu, P.X. Han, S.M. Dong, C.J. Zhang, J.H. Yao, G.L. Cui and L.Q. Chen, *J. Mater. Chem.*, 21 (2011) 11916.
19. W.Q. Mao, J.M. Wang, Z.H. Xu, Z.X. Niu and J.Q. Zhang, *Electrochem. Commun.*, 8 (2006) 1326.
20. T. Kuila, S. Bose, P. Khanra, A.K. Mishra, N.H. Kim and J.H. Lee, *Carbon*, 50 (2012) 914.
21. T.K. Zhao, W.B. Jin, Y.X. Wang, X.L. Ji, H.B. Yan, M. Khan, Y.T. Jiang, A. Dang, H. Li and T.H. Li, *Mater. Res. Lett.*, 212 (2018) 1.
22. M.L. Fang, Z. Wang, X.J. Chen and S.Y.Guan, *Appl. Surf. Sci.*, 436 **(**2018) 345.
23. K. Kakae, K. Hasanpour, *J. Mater. Chem. A*, 2 **(**2014**)** 15428**.**
24. D. Hulicova-Jurcakova, M. Seredych, G.Q. Lu and T.J. Bandosz, *Adv. Funct. Mater.*, 19 (2009) 438.
25. G. Abdi, A. Alizadeh and M.M. Khodaei, *Mater. Chem. Phys.*, 201 (2017) 323.
26. H.J. Zhang, B. Li, J.F. Pan, Y.W. Qi, J.N. Shen, C.J. Gao and B.J. Van der Bruggen, J. *Membrane. Sci.*, 539 (2017) 128.
27. S.L. Kuo, W.R. Liu, C.P. Kuo, N.L. Wu and H.C. Wu, *J. Power Sources*, 244 (2013) 552.
28. Y. Jiang, Z.J. Jiang, L.F. Yang, S. Cheng and M.L. Liu, *J. Mater. Chem. A*, 3 (2015) 11847.
29. Y.H. Lu, J.C. Hao, G.Y. Xiao, L. Chen, T.H. Wang and Z.Z. Hu, *Appl. Surf. Sci.*, 422 (2017) 710.
30. Z.S. Wu, W.C. Ren, L. Xu, F. Li and H.M. Cheng, *ACS Nano*, 5 (2011) 5463.

31. G.X. Wang, X.P. Sh en, J. Yao and J. Park, *Carbon*, 47 (2009) 2049.
32. S.L. Chou, Y. Zhao, J.Z. Wang, Z.X. Chen, H.K. Liu and S.X. Dou, *J. Phys. Chem. C*, 114 (2010) 15862.
33. S.W. Lee, N. Yabuuchi, B.M. Gallant, S. Chen, B.S. Kim, P.T. Hammond and Y. Shao-Horn, *Nat. Nanotechnol.*, 5 (2010) 531.